Multi-subject Orthogonal Sparse Matrix Decomposition Method for Extracting Individual Brain Functional Networks

Xingyu He[1], Vince D. Calhoun[2], Theo G.M. van Erp[3,4], and Yuhui Du[1*]

[1] School of Computer and Information Technology, Shanxi University, Taiyuan, 030006, China
[2] Tri-Institutional Center for Translational Research in Neuroimaging and Data Science (TReNDS), Georgia State University, Georgia Institute of Technology, Emory University, Atlanta, GA, 30030, USA
[3] Department of Psychiatry and Human Behavior, School of Medicine, University of California, Irvine, CA 92617 USA
[4] Center for the Neurobiology of Learning and Memory, University of California, Irvine, CA 92617 USA
duyuhui@sxu.edu.cn

Abstract. Brain functional network (FN) extraction is fundamental to advancing our understanding of brain function, providing critical insights into the neural mechanisms underlying cognition and behavior. Data-driven FN analysis methods have been developed to analyze functional magnetic resonance imaging (fMRI) data. However, to ensure cross-subject correspondence, group-level analyses of these methods sacrifice subject-specific variation. This trade-off between group-level alignment and subject-specific discrepancies hinders the accurate characterization of individual brain FNs. In this study, we propose a multi-subject orthogonal sparse matrix decomposition method without the need for group-level analysis, which simultaneously extracts both group-level FNs and individual FNs with cross-subject correspondence. We introduce a novel quasi-orthogonality constraint that enhances the linear independence of FNs, ensuring effective extraction of FNs, while enabling precise control over FN spatial scale. Additionally, by further incorporating a sparsity constraint, our method effectively minimizes spatial overlap between FNs, resulting in sparse representations. For simulated datasets, our method outperforms comparison methods, supporting its low parameter sensitivity and superior ability to extract FNs and time courses. Application to multi-site fMRI datasets, comprising 233 healthy controls (HCs) and 205 schizophrenia patients (SZs), validates the reproducibility of FNs extracted by our method. The results underscore the method's ability to preserve both cross-subject correspondence and individual variability. Overall, our method advances fMRI analytic capabilities by reconciling population-level consistency with individualized neural signatures, offering enhanced discriminative power for investigating neuropsychiatric disorder mechanisms and brain function.

Keywords: Functional Magnetic Resonance Imaging, Schizophrenia, Multi-subject Matrix Decomposition.

1 Introduction

The human brain, as a highly complex neurobiological system, governs fundamental cognitive processes including sensory perception, higher-order cognition, memory consolidation, and behavioral regulation [1]. Resting-state functional magnetic resonance imaging (fMRI) provides a whole-brain mapping of intrinsic neural activity. Building upon this methodological foundation, the data-driven functional network (FN) analysis method can identify spatially coherent neural ensembles and delineate their temporally synchronized activation patterns, thereby elucidating brain function [2].

The significance of individual differences in brain FNs highlights the necessity for methodologies that can both accommodate these variations and ensure cross-subject consistency [3, 4]. Three primary paradigms are commonly employed to analyze individual differences while ensuring inter-subject correspondence. The first paradigm employs single-subject FN analysis followed by post-hoc cross-subject alignment through clustering or matching procedures [5-7]. However, this approach may overemphasize subject-specific characteristics, leading to a lack of comparability of individual FNs. The second paradigm utilizes group-level FNs or existing templates as references for individual optimization, such as PCA-based methods [8], spatiotemporal (dual) regression [9], and group information-guided ICA (GIG-ICA) [10]. However, these methods may lead to individual FNs that are overly aligned with references [4]. The third paradigm directly enforces cross-subject correspondence during individual FN analysis. Independent vector analysis (IVA) [11-13] attempts to balance individual specificity and group consistency through cross-subject dependency modeling. Li et. al. incorporated an inter-subject group sparsity regularization term in non-negative matrix factorization (NMF) for enforcing individual FNs to common spatial structures [4]. Despite these advancements, the complex initialization processes in these methods may still interfere with the accurate representation of individual-specific information.

To capture individual variability while ensuring cross-subject correspondence, we propose a multi-subject orthogonal sparse matrix decomposition method for individual FN extraction. The primary contributions of this paper include: (1) Without requiring group-level analysis or complex initialization procedures, our proposed method enables concurrent identification of robust group-level FNs and individual FNs with cross-subject comparability. (2) We propose a novel quasi-orthogonality constraint that ensures the effective extraction of FNs by enhancing their linear independence while allowing for precise modulation of the FN scales. (3) By further incorporating a sparsity constraint, the proposed method effectively reduces the spatial overlap between FNs, yielding sparse representations. (4) The results on simulated datasets demonstrate the low parameter sensitivity and effectiveness of our proposed method in estimating individual FNs and time courses (TCs). Results on multi-site fMRI data validate the reproducibility of the FNs extracted by our method and indicate the cross-subject correspondence and individual variability of individual FNs.

2 Methods

2.1 Multi-Subject Orthogonal Sparse Matrix Decomposition Method for FMRI Data

Given an fMRI dataset $[X^1, X^2, \ldots, X^i, \ldots, X^m]$ consisting of m subjects, where $X^i \in \mathbb{R}^{s\times t}$ represents the ith subject's data matrix (with s voxels and t time points), the proposed multi-subject orthogonal sparse matrix decomposition method aims to simultaneously extract k group-level FNs $U_c \in \mathbb{R}^{s\times k}$, along with k subject-specific FNs $U^i \in \mathbb{R}^{s\times k}$ and corresponding TCs $V^i \in \mathbb{R}^{t\times k}$ for each subject i.

Given a single subject i, the sparse dictionary learning (SDL) as shown in (1) has been successfully applied to blind source separation problems, enabling effective FN extraction [14, 15].

$$\left\|X^i - U^i(V^i)^T\right\|_F^2 + \alpha\left\|U^i\right\|_1 \tag{1}$$

Here, α is used to regulate the sparsity of FNs. We extend the SDL method by incorporating the multi-view concept, which enables simultaneous multi-subject analysis while effectively preserving subject-specific information as formulated in (2).

$$\sum_{i=1}^{m}\left(\left\|X^i - U^i(V^i)^T\right\|_F^2 + \alpha\left\|U^i\right\|_1\right) \tag{2}$$

To establish the cross-subject correspondence of individual FNs, correspondence constraints $\beta\left\|U^i - U_c\right\|_F^2$ is used to align the individual FNs with the group-level FNs, as formulated in (3). By adjusting the parameter β, the degree of similarity between the individual FNs and the group-level FNs can be flexibly controlled. Moreover, (3) also contributes to improving the quality of the group-level FNs.

$$\sum_{i=1}^{m}\left(\left\|X^i - U^i(V^i)^T\right\|_F^2 + \alpha\left\|U^i\right\|_1 + \beta\left\|U^i - U_c\right\|_F^2\right) \tag{3}$$

To enhance the effectiveness of FN extraction, we impose an orthogonality constraint $(U^i)^T U^i = I$ as shown in (4). By enforcing orthogonality, the spatial separability among the extracted FNs can be significantly enhanced. The orthogonality constraint not only can reduce the spatial redundancy but also improve the reliability and interpretability of the FNs. In cases where orthogonality and sparsity constraints are incompatible, we strategically transfer the sparsity constraint to group-level FNs U_c, following the principles of self-supervised learning, to maintain the integrity and applicability of the method.

$$\sum_{i=1}^{m}\left(\left\|X^i - U^i(V^i)^T\right\|_F^2 + \beta\left\|U^i - U_c\right\|_F^2\right) + \alpha\|U_c\|_1, s.t.\,(U^i)^T U^i = I \tag{4}$$

To address the issue of excessively small FN scales induced by the orthogonality constraint, we propose a quasi-orthogonality constraint $(U^i)^T U^i = aI$ that not only preserves the orthogonality constraint's effect on spatial separation but also allows for flexible modulation of FN scales. Here, the scaling coefficient a enables systematic regulation of FN magnitudes.

Finally, the multi-subject sparse matrix decomposition method is formed as shown

in (5), enabling the simultaneous identification of robust group-level FNs and less-spatially overlapping, sparse, individual FNs with cross-subject correspondence.

$$\sum_{i=1}^{m}\left(\left\|X^i - U^i(V^i)^T\right\|_F^2 + \beta\left\|U^i - U_c\right\|_F^2\right) + \alpha\|U_c\|_1 \ s.t.\,(U^i)^T U^i = aI \tag{5}$$

2.2 Optimization

As shown in **Table 1**, the optimization process of our method includes initialization with k-means [16] and iterative optimization of the individual FNs U^i, their corresponding TCs V^i, and the group-level FNs U_c.

Given a subject i with fixing U_c, the optimization of V^i and U^i are completed. Equation (5) can be rewritten as Equation (6), and Equation (7) is used to update V^i by direct calculation.

$$min\left\|X^i - U^i(V^i)^T\right\|_F^2 + \beta\left\|U^i - U_c\right\|_F^2 \ s.t.\,(U^i)^T U^i = aI \tag{6}$$

$$V^i = {X^i}^T pinv((U^i)^T) \tag{7}$$

The updated rule of U^i is $U^i = \sqrt{a}\tilde{U}\tilde{V}^T$, where $\tilde{U}D\tilde{V}^T = svd(\sqrt{a}X^iV^i + \beta\sqrt{a}U_c)$, $svd(\cdot)$ represents the singular value decomposition operator. Prove as follows: (6) is rewritten as

$$\begin{aligned}\min_{(U^i)^T U^i = aI} & Tr((X^i)^T X^i - 2(X^i)^T U^i (V^i)^T + V^i (U^i)^T U^i (V^i)^T + \beta (U^i)^T U^i \\ & - 2\beta (U^i)^T U_c + \beta U_c^T U_c) \\ = \max_{(U^i)^T U^i = aI} & Tr((X^i)^T U^i (V^i)^T + \beta (U^i)^T U_c) \quad \text{let } H = \tfrac{1}{\sqrt{a}} U^i \\ = \max_{H^T H = I} & Tr\left(\sqrt{a}(X^i)^T H (V^i)^T + \beta\sqrt{a} H^T U_c\right).\end{aligned} \tag{8}$$

Combined with $\tilde{U}D\tilde{V}^T = svd(\sqrt{a}X^iV^i + \beta\sqrt{a}U_c)$,

$$\begin{aligned}Tr\left(\sqrt{a}(X^i)^T H (V^i)^T + \beta\sqrt{a} H^T U_c\right) &= Tr\left(\sqrt{a}X^i V^i H^T + \beta\sqrt{a} U_c H^T\right) \\ &= Tr\left(\tilde{U}D\tilde{V}^T H^T\right) \quad \text{let } Q = H\tilde{V} \\ &= Tr\left(\tilde{U}DQ^T\right),\end{aligned} \tag{9}$$

where $Tr(\cdot)$ represents the trace operation. Since $\tilde{V}\tilde{V}^T = I$ and $H^T H = I$, $Q^T Q = I$. Denoting $\tilde{U} = [\tilde{u}_1, \dots, \tilde{u}_k] \in \mathbb{R}^{m\times k}$, $D = Diag(d_1, \dots, d_k) \in \mathbb{R}_+^{k\times k}$, $Q = [q_1, \dots, q_k] \in \mathbb{R}^{n\times k}$. According to the Cauchy-Schwarz inequality,

$$Tr\left(\tilde{U}DQ^T\right) \le \sum_{i=1}^{k} d_i \|\tilde{u}_i\|_2 \|q_i\|_2 = \sum_{i}^{k} d_i = Tr(D), \tag{10}$$

when $Q = \tilde{U}$, $Tr\left(Q^T\tilde{U}D\right)$ reaches its upper bound, $Q = \tilde{U} = H\tilde{V}$. Finally, based on $\tilde{V}\tilde{V}^T = I$, the optimization rule for H is expressed by (11). Combined with $H = \frac{1}{\sqrt{a}}U^i$ The optimization rule for H is expressed by (12).

$$H = H\tilde{V}\tilde{V}^T = \tilde{U}\tilde{V}^T = \frac{1}{\sqrt{a}}U^i \tag{11}$$

$$U^i = \sqrt{a}H = \sqrt{a}\tilde{U}\tilde{V}^T \tag{12}$$

Given U^i and V^i, $arg\,min\sum_{i=1}^{m}\left(\beta\left\|U^i - U_c\right\|_F^2\right) + \|U_c\|_1$ is used to update U_c. The

soft threshold method [17] is used as shown in Equation (13).

$$[U_c]_{jk} = sign(\left[\frac{\sum_{i=1}^{m} U^i}{m}\right]_{jk}) \cdot max(|\left[\frac{\sum_{i=1}^{m} U^i}{m}\right]_{jk}| - \frac{\alpha}{2}, 0), \quad (13)$$

where $[A]_{jk}^{i}$ represents the (j,k)th element of A, $sign(\cdot)$ stands for the symbolic operator, $|\cdot|$ represents the absolute value operation.

Table 1. Multi-subject orthogonal sparse matrix decomposition method.

Algorithm 1	
Input: all fMRI data $X = [X^1, X^2, \dots, X^i, \dots, X^m]$, the number of FNs k, the number of subjects m, the parameters α and β.	
Output: the group-level FNs U_c, the individual FNs U^i, and corresponding TCs V^i.	
Initialization	**For** $\boldsymbol{i = 1:m}$ Initialize V^i by k-means; $U^i = X^i pinv((V^i)^T)$; **End** $U_c = \frac{\sum_{i=1}^{m} U^i}{m}$;
Updating process	**Repeat** For $i = 1:m$ $V^i = X^{i^T} pinv((U^i)^T)$; $\tilde{U}D\tilde{V}^T = svd(\sqrt{a}X^iV^i + \sqrt{a}\beta U_c)$; $U^i = \sqrt{a}\tilde{U}\tilde{V}^T$; End $[U_c]_{jk} = sign(\left[\frac{\sum_{i=1}^{m} U^i}{m}\right]_{jk}) \cdot max(|\left[\frac{\sum_{i=1}^{m} U^i}{m}\right]_{jk}| - \frac{\alpha}{2}, 0)$; **Until convergence**

3 Materials and Experiments

3.1 Experiments on Simulated Datasets

Using the SimTB toolbox [18], we generated two simulated fMRI datasets with identical parameters: a training set (sim_train) for assessing parameter sensitivity and parameter tuning, as well as an evaluation set (sim_eval) for method validation. Each dataset contained 20 subjects' data with 150 time points per subject, formatted as 148×148 voxel matrices. These simulations were constructed through linear combinations of 20 ground truth FNs, incorporating inter-subject variability via spatial transformations (translations, rotations, and spreads). The data augmentation included Rician noise with contrast-to-noise ratio randomized across subjects within the 0.65-1.0 range.

To assess the parameter sensitivity and select optimal parameters, the parametric relationship between α/β values and FN accuracy on the sim_train dataset is evaluated. We systematically evaluated two hyperparameters (α and β) across discrete values within predefined ranges ($\alpha \in [0.001, 0.01, 0.1, 0.2, 0.4, 0.6, 0.8]$, and $\beta \in$

$[0.01, 0.1, 0.5, 1, 2, 5, 10]$) using the sim_train dataset. The optimal parameter combination was identified based on the highest mean FN accuracy across all subjects, quantified by aligning the extracted FNs with ground truth FNs using the Hungarian algorithm [19] based on Pearson correlation coefficients.

To conduct a comparative performance evaluation of the extracted FN and TC accuracy, we implemented four methodologies that directly enforce cross-subject correspondence during individual FN analysis. These methods, including our method, our degraded method, the IVA method [20, 21], and the NMF method [4], were conducted on the sim_eval dataset. Here, our degraded method represents our method (5) without the sparsity constraint on group-level FNs.

3.2 Experiments on Real FMRI Datasets

The resting-state fMRI data from the Function Biomedical Informatics Research Network (FBIRN)[1] [22] and the Centers of Biomedical Research Excellence (COBRE)[2] [23] were used to evaluate the reliability of our proposed method and explore the pathogenesis of SZs. All demographic information is presented in **Table 2**. The details of data preprocessing and the acquisition of a common mask on fMRI data are described in detail in [24]. Finally, we obtained fMRI data from three datasets, including the COBRE dataset with all 157 subjects from COBRE, the FBIRN_HC dataset with all 144 HCs from FBIRN, and the FBIRN_SZ dataset with all 137 SZs from FBIRN.

Table 2. Demographic information.

		Age mean±std	Gender male/female	Transition mean±std	Rotation mean±std
COBRE	**HCs**	38.09±11.66	64/25	0.22±0.15	0.19±0.12
	SZs	37.74±14.47	57/11	0.20±0.12	0.18±0.12
	p-value	0.8652	0.0785	0.3624	0.5258
FBIRN	**HCs**	37.15±11.00	104/40	0.19±0.15	0.21±0.16
	SZs	39.02±11.35	103/34	0.18±0.13	0.20±0.16
	p-value	0.1605	0.5733	0.4239	0.4223

Note: The two-sample t-test was used for investigating age and head movement differences between HCs and SZs, and the chi-square test was used for sex differences between HCs and SZs.

We applied the proposed method to three datasets (COBRE, FBIRN_HC, and FBIRN_SZ) to extract group-level FNs, individual FNs, and corresponding TCs, with the FN count fixed at 25, $\alpha = 0.1$, and $\beta = 1$.

To assess the reproducibility of the extracted FNs and examine the group-level differences between the HCs and SZs, we utilized the group-level FNs derived from the COBRE dataset as a reference to align all group-level FNs across all three sites as follows: (1) between COBRE and FBIRN_HC, (2) between COBRE and FBIRN_SZ. The matching processes were carried out using the Hungarian algorithm [19] with Pearson correlation coefficients. Only the FNs that exhibited stable matching with a single site

[1] https://doi.org/10.1016/j.neuroimage.2015.09.003

[2] http://fcon_1000.projects.nitrc.org/indi/retro/cobre.html

in both FBIRN_SZ and FBIRN_HC datasets were identified to reflect the differences of functional networks between HCs and SZs.

To further characterize cross-subject correspondence and individual variability, we randomly selected 10 subjects from the COBRE dataset and rearranged their individual FNs according to the order of group-level FNs. Then, the correlations between rearranged individual FNs are computed and presented.

4 Results

4.1 Results on Simulated Datasets

The relationship between α/β values and mean FN (TC) accuracy across all subjects in the sim_train dataset is illustrated in Fig. 1(A). Based on this analysis, α=0.1 and β=1 are selected as the optimal parameters. The results show that our proposed method maintains high accuracy in extracting both FNs and TCs across a wide range of parameter settings, indicating a robust performance with low sensitivity.

Fig. 1(B) shows the accuracy of the extracted FNs and TCs across four methods for all subjects in the sim_eval dataset. Our method demonstrates superior performance in FN extraction compared to the IVA and NMF methods while maintaining comparable accuracy to the IVA method in TC extraction. The FN (TC) extraction accuracy of our method achieves 0.9660 (0.9642), which is higher than the degraded method's accuracy of 0.9652 for FNs and 0.9641 for TCs. These results collectively highlight the robustness and effectiveness of our method in FN extraction.

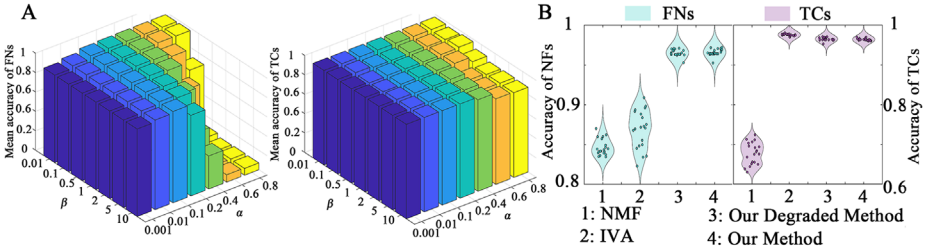

Fig. 1. Accuracy of individual FNs and TCs on simulated datasets. (A) The relationship between α/β values and mean FN (TC) accuracy across all subjects in the sim_train dataset. (B) Boxplots illustrating the accuracy of extracted FNs and TCs for all the simulated subjects in the sim_eval dataset. Four methods are compared: NMF, IVA, our degraded method, and our method.

4.2 Results of Real FMRI Datasets

Fig. 2(A) illustrates the correlation of group-level FNs between COBRE and FBIRN_HC (FBIRN_SZ). Of the 25 FNs extracted, 18 (20) group-level FNs exhibit correlations exceeding 0.5 between COBRE and FBIRN_HC (FBIRN_SZ). Three representative FNs, which are stably identified across all three datasets, along with their correlations, are displayed in Fig. 2(B). These findings collectively demonstrate the reproducibility of the group-level FNs extracted using our method.

From Fig. 2(A), we observe that FN 2 is reproducibly identified only in the COBRE and FBIRN_HC datasets, while FN 25 shows consistent identification exclusively in COBRE and FBIRN_SZ datasets, which suggests potential variability in the manifestation of FN 2 and FN 25 across schizophrenia populations. These two FNs, which are associated with the cerebellum and superior temporal gyrus, are highlighted in Fig. 2(C).

As shown in Fig. 2(D), all 25 group-level brain FNs from the COBRE dataset are summarized into a template, which highlights the spatial tightness and smoothness of the extracted FNs. Fig. 2(E) presents the correlations between rearranged individual FNs derived from 10 randomly selected subjects from the COBRE dataset. The observed strict block-diagonal structure, with distinct correlations within each block, underscores the method's ability to effectively identify subject-specific individual FNs while maintaining consistent cross-subject correspondence.

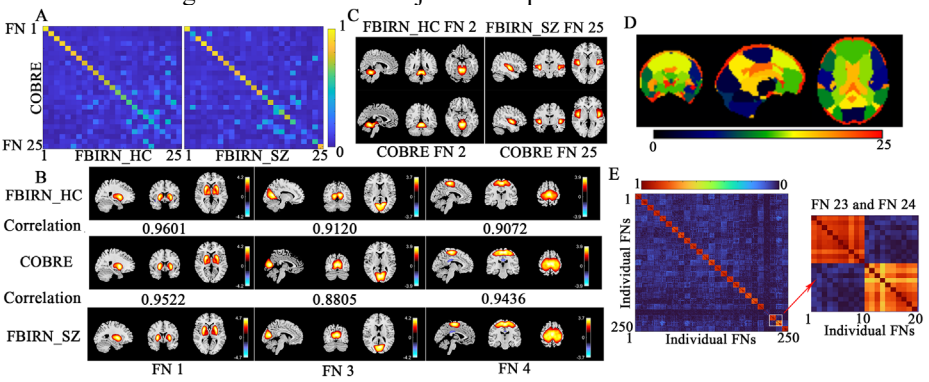

Fig. 2. Visualization of FNs and their correlation in real fMRI datasets. (A) Correlation of group-level FNs between COBRE and FBIRN_HC (FBIRN_SZ). (B) Display of three group-level FNs and their correlation value between COBRE and FBIRN_HC (FBIRN_SZ). (C) Two group-level FNs showing functional differences between HCs and SZs. (D) FN template derived from COBRE. (E) Correlations between the rearranged individual FNs of 10 random subjects.

5 Conclusion

This study proposes a novel multi-subject orthogonal sparse matrix decomposition method for functional network analysis, designed to concurrently extract group-level functional networks and individual functional networks with cross-subject correspondence, without requiring group-level analysis or complex initialization. Another key innovation lies in the introduction of a quasi-orthogonality regularization, which not only improves the linear independence of functional networks but also allows precise modulation of their scales. Furthermore, the incorporation of a sparsity constraint effectively minimizes spatial overlap between networks, resulting in sparse representations that enhance interpretability.

For simulated datasets, our method outperforms comparison methods, supporting its low parameter sensitivity and superior ability to extract functional networks and time courses. For multi-site fMRI datasets, the results validate the reproducibility of

networks extracted by our method and underscore the method's ability to preserve both cross-subject correspondence and individual variability. Additionally, the results from our method reveal differences in group-level functional networks between the healthy controls and schizophrenia patients, associated with the cerebellum and superior temporal gyrus. These findings align with previous studies that have highlighted functional abnormalities in schizophrenia populations [25, 26], thereby supporting the validity of our method. In summary, the proposed method represents a significant advancement in functional neuroimaging analysis research.

Acknowledgments. The work was supported by the National Natural Science Foundation of China (62076157 and 61703253, to Yuhui Du) and the National Institutes of Health (R01MH123610, to Vince D. Calhoun).

Disclosure of Interests. The authors have no competing interests to declare.

References

1. Sultana, O.F., et al., *Unraveling the complexity of human brain: Structure, function in healthy and disease states.* Ageing Research Reviews, 2024. **100**: p. 102414.
2. Du, Y., et al., *A survey of brain functional network extraction methods using fMRI data.* Trends in Neurosciences, 2024.
3. Kong, R., et al., *Spatial topography of individual-specific cortical networks predicts human cognition, personality, and emotion.* Cerebral cortex, 2019. **29**(6): p. 2533-2551.
4. Li, H., T.D. Satterthwaite, and Y. Fan, *Large-scale sparse functional networks from resting state fMRI.* Neuroimage, 2017. **156**: p. 1-13.
5. De Martino, F., et al., *Classification of fMRI independent components using IC-fingerprints and support vector machine classifiers.* Neuroimage, 2007. **34**(1): p. 177-194.
6. Esposito, F., et al., *Independent component analysis of fMRI group studies by self-organizing clustering.* Neuroimage, 2005. **25**(1): p. 193-205.
7. Yang, Z., et al., *Generalized RAICAR: discover homogeneous subject (sub) groups by reproducibility of their intrinsic connectivity networks.* Neuroimage, 2012. **63**(1): p. 403-414.
8. Calhoun, V.D., et al., *A method for making group inferences from functional MRI data using independent component analysis.* Human brain mapping, 2001. **14**(3): p. 140-151.
9. Beckmann, C.F., et al., *Group comparison of resting-state FMRI data using multi-subject ICA and dual regression.* Neuroimage, 2009. **47**(Suppl 1): p. S148.
10. Du, Y. and Y. Fan, *Group information guided ICA for fMRI data analysis.* Neuroimage, 2013. **69**: p. 157-197.
11. Kim, T., T. Eltoft, and T.-W. Lee. *Independent vector analysis: An extension of ICA to multivariate components*. in *International conference on independent component analysis and signal separation*. 2006. Springer.

12. Anderson, M., T. Adali, and X.-L. Li, *Joint blind source separation with multivariate Gaussian model: Algorithms and performance analysis.* IEEE Transactions on Signal Processing, 2011. **60**(4): p. 1672-1683.
13. Vu, T., et al., *Constrained independent vector analysis with reference for multi-subject fMRI analysis.* IEEE Transactions on Biomedical Engineering, 2024.
14. Bhanot, A., et al., *Spatially constrained online dictionary learning for source separation.* IEEE Transactions on Image Processing, 2021. **30**: p. 3217-3228.
15. Seghouane, A.-K. and A. Iqbal, *Basis expansion approaches for regularized sequential dictionary learning algorithms with enforced sparsity for fMRI data analysis.* IEEE transactions on medical imaging, 2017. **36**(9): p. 1796-1807.
16. Ding, C.H., T. Li, and M.I. Jordan, *Convex and semi-nonnegative matrix factorizations.* IEEE transactions on pattern analysis and machine intelligence, 2008. **32**(1): p. 45-55.
17. Beck, A. and M. Teboulle, *A fast iterative shrinkage-thresholding algorithm for linear inverse problems.* SIAM journal on imaging sciences, 2009. **2**(1): p. 183-202.
18. Erhardt, E.B., et al., *SimTB, a simulation toolbox for fMRI data under a model of spatiotemporal separability.* Neuroimage, 2012. **59**(4): p. 4160-4167.
19. Carpaneto, G. and P. Toth, *Algorithm 548: Solution of the assignment problem [H].* ACM Transactions on Mathematical Software (TOMS), 1980. **6**(1): p. 104-111.
20. Lee, J.-H., et al., *Independent vector analysis (IVA): multivariate approach for fMRI group study.* Neuroimage, 2008. **40**(1): p. 86-109.
21. Luo, Z., *Independent vector analysis: Model, applications, challenges.* Pattern Recognition, 2023. **138**: p. 109376.
22. Keator, D.B., et al., *The function biomedical informatics research network data repository.* Neuroimage, 2016. **124**: p. 1074-1079.
23. Aine, C., et al., *Multimodal neuroimaging in schizophrenia: description and dissemination.* Neuroinformatics, 2017. **15**: p. 343-364.
24. He, X., V.D. Calhoun, and Y. Du, *SMART (splitting-merging assisted reliable) Independent Component Analysis for Extracting Accurate Brain Functional Networks.* Neuroscience Bulletin, 2024: p. 1-16.
25. Ferri, J., et al., *Resting-state thalamic dysconnectivity in schizophrenia and relationships with symptoms.* Psychological medicine, 2018. **48**(15): p. 2492-2499.
26. Xing, Y., et al., *A novel neighborhood rough set-based feature selection method and its application to biomarker identification of schizophrenia.* IEEE journal of biomedical and health informatics, 2022. **27**(1): p. 215-226.